Training method for refinement of machine-learning interatomic potential and its applications

Kohei Shimamura, Akihide Koura, and Fuyuki Shimojo
Department of Physics, Kumamoto University,
Kumamoto 860-8555, Japan

Abstract

Machine-learning interatomic potential (MLIP) is based on low-cost ML models trained with first-principles data to achieve high accuracy in molecular dynamics simulations, expanding the range of applicable time-space domains. However, the current widely used training method has limitations in accurately estimating stress and fundamental physical quantities such as free energy and thermal conductivity. We have therefore emphasized the importance of stress training for MLIPs and investigated other issues behind the current training method. The report discusses the role of stress training in reproducing solid-liquid phase transitions and estimating thermal conductivity, as well as the effect of training data with different k points on free energy.

1 Introduction

The machine-learning interatomic potential (MLIP) is used in a wide range of research fields. By training low-cost machine learning models with first-principles molecular dynamics (FPMD) data, the MLIP achieves high accuracy, significantly expanding the applicable space-time domain of MD simulations. MLIP is used to calculate physical quantities that require large statistical amounts, to investigate phenomena occurring in long-term dynamic simulations such as shock waves, and to explore reaction pathways [1, 2, 3].

Under these circumstances, we have been working on the refining the training method of MLIPs. In particular, we have emphasized the importance of stress training to MLIP [4, 5]. Recent mainstream training methods set total potential energy and atomic force as the targets in training [6]. Despite the fact that the accuracy of stress is not guaranteed, some previous studies to investigate high-pressure phenomena have utilized such MLIPs. It is moreover found that the stress training is necessary to accurately estimate fundamental physical quantities such as thermal conductivity (TC), and becomes one of the indispensable training conditions [5]. This report discusses the importance of stress training of MLIPs for reproducing a phase transition and estimating TC. In addition, we also discuss the effect of training data with different k points on thermodynamic quantities obtained through MLIPs, such as free energy. As the MLIP, we adopted an interatomic potential using an artificial neural network (ANN potential).

1.1 Stress training

Originally MLIPs were trained with only total potential energy. Afterward, atomic force, which is crucial for MD simulations, was integrated into the training process, leading to a significant improvement in accuracy compared to MLIPs that only consider the total potential energy. Recently, some MLIPs have been obtained by training with FP data of the total potential energy, atomic force, and stress. However, such MLIPs that target stress in training may still be in a minority. In this report, we show our results that the accuracy of stress is not guaranteed by training with the total potential

energy and atomic force alone, and that the solid-liquid phase transition of Na is accurately reproduced by training with stress [4].

1.2 Free energy calculation

Thermodynamic integration (TI) is a popular method for computing free energy, but when combined with MLIPs such as ANN potentials, some considerations need to be taken for liquids. We discovered a method that involved two steps, using an ideal gas and a soft potential as reference systems [7]. We show how to calculate the free energies of solid and liquid states by the TI method using ANN potential for Na [4].

Furthermore, in numerous previous studies, MLIPs were trained using FP data with multiple k points instead of using of large-scale systems. We however show that as precision requirements increase, larger systems with a greater number of k points will be necessary for the free energy calculation [4].

1.3 TC calculation

The TC calculation method based on the Green-Kubo (GK) formula has been widely used because it can be applied to even disordered systems. However, MLIPs including the ANN potential belong to many-body potentials, and the many-body effects have to be taken into account in the formula of the heat flux [8]. We found that using the rigorous heat flux formula considering the effects together with applying stress training to the ANN potential led to highly accurate TC estimates [9]. Here, we show the result of the TC for the superionic conducting Ag_2Se (α-Ag_2Se) by homogeneous nonequilibrium MD (HNEMD) based on the GK formula [9].

2 Computational Details

In this study, FPMD and MD simulations using MLIPs were conducted using the QXMD code [10].

2.1 ANN potential

The ANN potentials were constructed using ænet [11], which is a training code developed by Artrith *et al.* The ANN potential comprises feed forward neural networks (FFNNs) created for each atomic species. The total potential energy U^{ANN} is defined by the sum of the atomic potential energies $\{\varepsilon_i^{\mathrm{ANN}}\}$ output from FFNNs for all atoms in the system [12].

$$U^{\mathrm{ANN}} = \sum_i^{N_{\mathrm{atom}}} \varepsilon_i^{\mathrm{ANN}}, \tag{1}$$

where N_{atom} denotes the total number of atoms.

The atomic potential energy depends on the structural descriptor used. Chebyshev descriptors [13] were used in this study. The atomic potential energy of the Chebyshev descriptor is only a function of the relative coordinates $\mathbf{r}_{ij}$ [5]

$$\varepsilon_i^{\mathrm{ANN}} = \varepsilon_i^{\mathrm{ANN}}\left(\{\mathbf{r}_{ij}\}_{j\neq i}\right). \tag{2}$$

2.2 Training methods

The following cost function C was used to train the ANN potentials. It consists of three loss functions, i.e., the total potential energy, atomic force, and virial.

$$\begin{aligned} C &= \frac{p_U}{2}\frac{1}{N_I}\sum_I^{N_I}\left(\frac{U_I^{\mathrm{ANN}}-U_I^{\mathrm{Ref}}}{N_{\mathrm{atom}}}\right)^2 \\ &+ \frac{p_F}{2}\frac{1}{N_I}\sum_I^{N_I}\frac{1}{3N_{\mathrm{atom}}}\sum_i^{N_{\mathrm{atom}}}\left(\mathbf{F}_{I,i}^{\mathrm{ANN}}-\mathbf{F}_{I,i}^{\mathrm{Ref}}\right)^2 \\ &+ \frac{p_W}{2}\frac{1}{N_I}\sum_I^{N_I}\frac{1}{6}\sum_j^{6}\left(\frac{W_{I,j}^{\mathrm{ANN}}-W_{I,j}^{\mathrm{Ref}}}{N_{\mathrm{atom}}}\right)^2, \end{aligned} \tag{3}$$

where N_I denotes the number of training data. The symbol "Ref" denotes the training data. Factor 6 for the virial term reflects the number of independent degrees of freedom of the virial tensor $\mathrm{W}_I^{\mathrm{ANN}}$. Because the three loss functions differ in dimension and size, p_U, p_F, and p_W are introduced as adjustable parameters. With appropriate settings of these parameters, highly accurate ANN potentials can be constructed [14].

Note that the training for virial tensor $\mathrm{W}_I^{\mathrm{ANN}}$ is equivalent to that for the stress tensor $\mathrm{P}_I^{\mathrm{ANN}}$ calculated by dividing $\mathrm{W}_I^{\mathrm{ANN}}$ by supercell volume.

The ANN potential trained with total potential energy and atomic force is called EF-fit, while the one trained including virial is called EFP-fit.

2.3 Generation of training data on Na

We obtained the training data of Na by running FPMD simulations. We calculated the electronic states using the projector-augmented-wave (PAW) method [15] within the framework of density functional theory (DFT) [16], in which the generalized gradient approximation (GGA) [17] was used for the exchange-correlation energy. The plane-wave cutoff energies were 10 and 50 Ry for the electronic pseudo-wave functions and pseudo-charge density, respectively. Projector functions were generated for the $3s$, $3p$, and $3d$ state of Na atom.

The FPMD simulations were mainly performed using 128 Na atoms with periodic boundary conditions. For the Brillouin-zone sampling, 4 and 32 special k points were utilized in addition to the Γ point. These are equivalent to sampling at the Γ point in systems consisting of 1024 and 8192 atoms, respectively. For comparison, FPMD simulations were also conducted on 1024 Na atoms using the Γ point. The equations of motion were solved under the isothermal-isobaric (NPT) ensemble through an explicit reversible integrator [18]. The pressure was set to be ambient. The MD time step Δt was 2.9 fs. The simulation temperature was mainly set to 350 K. In addition, FPMD data using 128 atoms with Γ point were prepared for heating and cooling processes in the range between 450 and 200 K to investigate whether the ANN potential can reproduce the melting and solidification processes of Na.

2.4 TI method

In the TI method [4, 7], the interaction energy $U(\lambda)$ with parameter λ and the Helmholtz free energy $F(\lambda)$ are connected by the following relation:

$$\frac{\partial F(\lambda)}{\partial \lambda} = \left\langle \frac{\partial U(\lambda)}{\partial \lambda} \right\rangle_{NVT}, \tag{4}$$

where $\langle \cdots \rangle_{NVT}$ denotes the canonical (NVT) ensemble average. $U(\lambda)$ is given as

$$U(\lambda) = \lambda U_{\mathrm{Na}} + (1-\lambda) U_{\mathrm{ref}} \ \ (0 \le \lambda \le 1), \tag{5}$$

where U_{Na} and U_{ref} are the total potential energies of the target (Na) and reference systems, respectively. By substituting Eq. (5) into Eq. (4), and integrating both sides with respect to λ from 0 to 1, we obtain the following formula:

$$F(\lambda=1) - F(\lambda=0) = \int_0^1 \langle U_{\mathrm{Na}} - U_{\mathrm{Ref}} \rangle_{NVT} \, d\lambda. \tag{6}$$

$F(\lambda=1)$ and $F(\lambda=0)$ are the free energies of the target and reference systems, respectively. As reference systems for the solid and liquid phases, we employed an Einstein solid and an ideal gas, respectively.

In the liquid phase, the soft core (SC) potential U_{SC}, defined as follows, was employed to avoid shortening the interatomic distance as λ approaches zero [7].

$$U_{\mathrm{SC}}(\{\boldsymbol{r}_i\}) = \sum_{i<j}^{N} \mu \left(\frac{\sigma}{r_{ij}} \right)^n. \tag{7}$$

The parameters were used to be $\mu = 7.92 \times 10^{-4}$ hartree, $\sigma = 6.752$ bohr, and $n = 12$. The Helmholtz free energy in the liquid phase was calculated by two TIs. The first TI is calculated along the ideal gas to SC liquid and the second one is from SC to the target liquid Na. In addition, to integrate the first while preventing divergence at smaller λ, we adopted the coordinate transformation from λ to x proposed in the previous study [19]

$$\lambda(x) = \left(\frac{x+1}{2} \right)^{\frac{1}{1-k}}, \tag{8}$$

where the interval of integration is changed from $0 \le \lambda \le 1$ to $-1 \le x \le 1$. We employed the parameter $k = 0.85$. Applying this transformation to the integration with respect to λ, we have the following formula:

$$\int_0^1 f(\lambda) d\lambda = \frac{1}{2(1-k)} \int_{-1}^{1} f(\lambda(x)) \lambda(x)^k dx \,. \tag{9}$$

2.5 Generation of training data on α-Ag_2Se

We generated training data using MD simulations with an empirical interatomic potential (EIP) instead of FPMD. One reason for this is that we can obtain a reference value of TC. The other reason is that the EIP of Ag_2Se proposed by Rino *et al*. [20] is a physically excellent EIP that can describe phase transitions among nonsuperionic, superionic conducting, and liquid phases [21]. The training data were obtained by MD simulation with the NVT ensemble at 500 K for the α-Ag_2Se system that comprises 256 Ag + 128 Se atoms in experimental density [22].

2.6 TC calculation

2.6.1 GK formula and heat flux

According to the GK formula [23, 24], the $\alpha\beta$ component of the TC tensor $\kappa_{\alpha\beta}$ can be estimated as ($\alpha, \beta \in \{x, y, z\}$)

$$\kappa_{\alpha\beta} = \frac{\Omega}{k_{\mathrm{B}}T^2}\int_0^\infty \langle J_{Q,\alpha}(t)J_{Q,\beta}(0)\rangle dt, \quad (10)$$

where T, k_{B}, and Ω are temperature, the Boltzmann constant, and volume of the supercell, respectively. $\langle J_{Q,\alpha}(t)J_{Q,\beta}(0)\rangle$ denotes the auto-correlation function of the heat flux $\mathbf{J}_Q$, and the following expression is employed for both the EIP and ANN potentials:

$$\mathbf{J}_Q = \frac{1}{\Omega}\sum_i^{N_{\mathrm{atom}}} t_i\mathbf{v}_i + \frac{1}{\Omega}\sum_i^{N_{\mathrm{atom}}} \varepsilon_i\mathbf{v}_i + \frac{1}{\Omega}\sum_i^{N_{\mathrm{atom}}} \mathrm{W}_i\mathbf{v}_i \quad , \quad (11)$$

where t_i, $\mathbf{v}_i$, ε_i, and W_i are atomic kinetic energy, velocity, potential energy, and virial tensor for the ith atom, respectively.

2.6.2 Atomic virials in heat flux formula

To derive a rigorous formula of the heat flux for the many-body potentials, an expression for the atomic potential energy is required [8], which corresponds to Eq. (2) for the ANN potentials. In our previous study [5], we have succeeded in deriving the heat flux formula and showed that the atomic virial is expressed as follows.

$$\mathrm{W}_i^{\text{ANN-I}} = \sum_{j\neq i}\mathbf{r}_{ij}\otimes\frac{\partial\varepsilon_j^{\mathrm{ANN}}}{\partial\mathbf{r}_{ji}}. \quad (12)$$

Incidentally, for the many-body potentials such as the ANN potential, there are countless definitions of atomic virial which give identical total virials [9, 5]. We define two more apparently reasonable atomic virials used for heat fluxes in the previous studies.

$$\mathrm{W}_i^{\text{ANN-II}} = \sum_{j\neq i}\mathbf{r}_{ij}\otimes\frac{\partial\varepsilon_i^{\mathrm{ANN}}}{\partial\mathbf{r}_{ji}}, \quad (13)$$

and

$$\mathrm{W}_i^{\text{ANN-III}} = \frac{1}{2}\sum_{j\neq i}\mathbf{r}_{ij}\otimes\left[\frac{\partial\varepsilon_i^{\mathrm{ANN}}}{\partial\mathbf{r}_{ji}} + \frac{\partial\varepsilon_j^{\mathrm{ANN}}}{\partial\mathbf{r}_{ji}}\right]. \quad (14)$$

$\mathrm{W}_i^{\text{ANN-II}}$ appears naturally in the stress-tensor derivation for the ANN potentials [25]. In Ref. [26], $\mathrm{W}_i^{\text{ANN-III}}$ was used because the pairwise force defined as $\mathbf{F}_{ij}^{\mathrm{ANN}} = -\left[\frac{\partial\varepsilon_i^{\mathrm{ANN}}}{\partial\mathbf{r}_{ji}} + \frac{\partial\varepsilon_j^{\mathrm{ANN}}}{\partial\mathbf{r}_{ji}}\right]$ satisfies Newton's third law [8]. The summation $\sum_j^{N_{\mathrm{atom}}}\mathbf{F}_{ij}^{\mathrm{ANN}}$ is equal to $\mathbf{F}_i^{\mathrm{ANN}}$. While the mathematical properties of the three atomic virials differ, their sums over N_{atom} yield the same total virial $\mathrm{W}^{\mathrm{ANN}}$. Hereinafter, the heat flux formulae defined by substituting $\mathrm{W}_i^{\text{ANN-I}}$, $\mathrm{W}_i^{\text{ANN-II}}$, and $\mathrm{W}_i^{\text{ANN-III}}$ into Eq. (11) are referred to as $\mathbf{J}_Q^{\mathrm{I}}$, $\mathbf{J}_Q^{\mathrm{II}}$, and $\mathbf{J}_Q^{\mathrm{III}}$, respectively. Some studies used ANN potentials that estimated TCs with $\mathbf{J}_Q^{\mathrm{II}}$ [27] and $\mathbf{J}_Q^{\mathrm{III}}$ [26]. Recent studies highlighted that the atomic virial can significantly impact the TC when dealing with many-body potentials [8, 28, 29]. It is crucial to compare the TCs obtained from these heat flux formulae.

2.6.3 HNEMD method

The HNEMD method [30], which is based on the GK formula, has successfully reduced the computational cost by enabling the calculation of TC using the time average of the heat flux instead of integrating its auto-correlation function.

$$\kappa = \frac{\Omega}{F_{\mathrm{ext}}T}\lim_{t\to\infty}\langle J_{Q,x}\rangle_t, \quad (15)$$

where F_{ext} denotes a magnitude of perturbation along the x direction of the system. F_{ext} = 0.01 bohr^{-1} was selected for the HNEMD simulations in this study [5].

3 Results

3.1 Solid-liquid phase transition of Na

We first investigated whether the EF-fit and EFP-fit models reproduced the hysteresis of melting and solidification in Na [4]. These two types of ANN potentials were constructed from the FPMD data in the temperature range of 200 to 450 K, performed using 128 atoms with Γ point as mentioned in section 2.3. The EFP-fit was able to accurately reproduce the heating and cooling processes of FPMD. The temperature dependence of radial distribution function $g(r)$ obtained from the MD simulations is shown in Fig. 1. $g(r)$'s by the EFP-fit (green dashed lines) are quite consistent with the FPMD results (black solid lines). In contrast, the $g(r)$ obtained from the MD simulations using EF-fit (red dashed lines) showed a significant deviation from those obtained from FPMD . The above results demonstrate the risk by using MLIPs such as EF-fit, which do not guarantee the accuracy of stress.

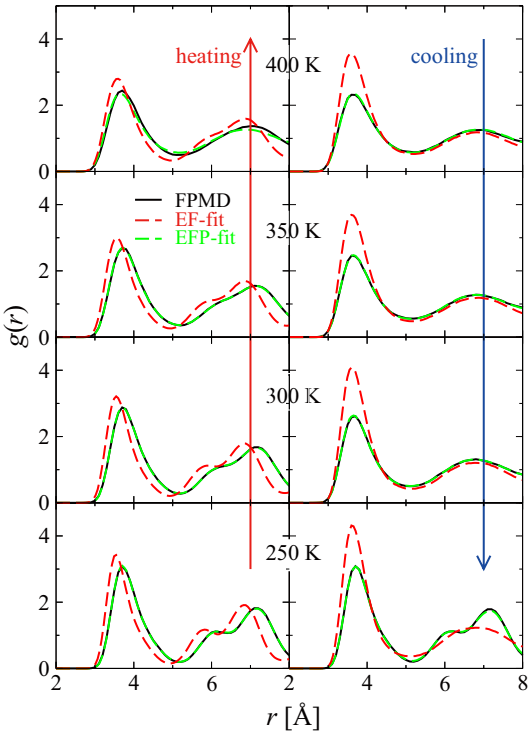

Figure 1: Temperature dependence of the radial distribution function $g(r)$ in the heating and cooling processes. The black solid lines correspond to the results from FPMD simulations. The red and green dashed lines correspond to those from MD simulations with EF-fit and EFP-fit, respectively. Taken from Ref. [4].

3.2 Size dependence of the free energy of Na

In many previous studies, the training data of MLIPs were created by FP calculation with many k points to avoid using large-scale systems. However, it is not obvious whether the respective MLIPs constructed from the training data obtained with a specific number of k points and corresponding system sizes show equivalent accuracy. Therefore, we conducted the following analysis to clarify the influence of training conditions such as system size and the number of k points on thermodynamic quantities such as free energy [4].

We created the four types of EFP-fit models. These were trained with the FPMD data obtained from the 128-atom system with Γ point, 128-atom system with 4k points, 128-atom system with 32k points, and 1024-atom system with Γ point, which are hereinafter referred to as 128-ΓANN, 128-4kANN, 128-32kANN, and 1024-ΓANN potentials, respectively. To investigate the size-dependent behavior of thermodynamic quantities, we calculated the Helmholtz free energy for 128 and 1024 atoms using 128-ΓANN and 128-4kANN potentials. Additionally, for comparison, we computed the same quantities for 1024 atoms using 1024-ΓANN and 128-32kANN potentials. Figure 2 shows the (a) Helmholtz free energy F, (b) total potential energy U, and (c) product of entropy and temperature TS as a function of the number of atoms N. The triangles and circles represent the solid and liquid phases, respectively. The black, red, green, and blue symbols de-

note the values calculated using the 1024-ΓANN, 128-4kANN, 128-ΓANN, and 128-32kANN potentials, respectively. As observed from this figure, the outcomes obtained using the128-ΓANN potential exhibit significant deviation from the others. Moreover, the values computed using the 1024-ΓANN, 128-4kANN, and 128-32kANN potentials are nearly identical with regard to the vertical axis.

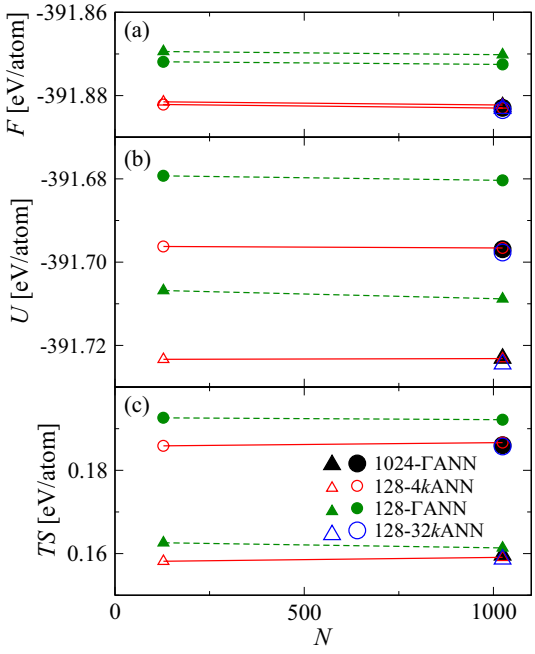

Figure 2: (a) Helmholtz free energy F, (b) total potential energy U, and (c) product of entropy and temperature TS obtained using the TI method at 350 K as a function of the number of atoms N. Triangles and circles correspond to the solid and liquid states, respectively. The black, red, green, and blue symbols indicate the values calculated using the 1024-ΓANN, 128-4kANN, 128-ΓANN, and 128-32kANN potentials, respectively. Taken from Ref. [4].

To further examine the size dependence, we computed the differences in Helmholtz free energy between the solid and liquid states $\Delta F = F_{\rm liq} - F_{\rm sol}$, as shown in Table 1. From the table, we obtained the following findings: (i) the values obtained from the 128-ΓANN potential differs largely from the others; (ii) the difference in ΔF between 128 and 1024 atoms is merely 0.13 and 0.11 meV/atom when calculated with the 128-ΓANN and 128-4kANN, respectively, suggesting that for systems with more than 128 atoms, the size dependence on ΔF is almost negligible in comparison with the difference of Helmholtz free energy; (iii) the difference between the ΔF values computed using the128-4kANN and 1024-ΓANN potentials is relatively small, with a difference of only 0.50 meV/atom for 1024 atoms; (iv) the value of ΔF obtained using the 128-32kANN is more similar to that obtained using the 1024-ΓANN than to that obtained using the 128-4kANN. Despite being trained with FPMD data at a single temperature of 350 K, the 128-4kANN potential is capable of accurately calculating ΔF with an error of only a few tenths of meV/atom. However, if higher precision is required, larger systems with more k points will be necessary.

Table 1: Differences of Helmholtz free energy $\Delta F = F_{\rm liq} - F_{\rm sol}$ between the solid and liquid states at 350 K in meV/atom. Taken from Ref. [4]

Atoms	128-Γ	128-4k	1024-Γ	128-32k
128	-2.47	-0.63	-	-
1024	-2.34	-0.74	-0.24	-0.33

3.3 TC calculation of α-Ag_2Se

The stress training is also associated with the accuracy of TC. Here, we present the results of an investigation of the influence of the heat flux formulae ($\mathbf{J}^{\rm I}_Q$, $\mathbf{J}^{\rm II}_Q$, and $\mathbf{J}^{\rm III}_Q$) and stress training on TC, using α-Ag_2Se as the test system [5].

To examine the effect of stress training, we used the EF-fit and EFP-fit models, and also took into account the dependence of the initial weight parameters in ANN. We constructed five each of the EF-fit and EFP-fit with different initial weight parameters. Figure 3 plots five TCs ($\kappa^{\rm ANN}$) obtained from the respective EF-fit and EFP-fit models as a function of root mean square errors of stress for the validation data ($\Delta P_{\rm valid}$). The vertical axis shows the absolute value $|\kappa^{\rm ANN} - \kappa^{\rm EIP}|$,

where κ^{EIP} is the reference TC obtained from the EIP (0.274 $\mathrm{Wm^{-1}K^{-1}}$). For the EF-fit, while three TCs calculated by $\mathbf{J}^{\mathrm{I}}_Q$ are sufficiently close to 0, all of the five $\Delta P_{\mathrm{valid}}$ are larger than 0.47 GPa. Furthermore, $|\kappa^{\mathrm{ANN}} - \kappa^{\mathrm{EIP}}|$ exhibits a large value of ~ 0.2 $\mathrm{Wm^{-1}K^{-1}}$ with higher values of $\Delta P_{\mathrm{valid}}$ when using $\mathbf{J}^{\mathrm{I}}_Q$. $\mathbf{J}^{\mathrm{II}}_Q$ gives large errors of the TCs $\sim$0.25 $\mathrm{Wm^{-1}K^{-1}}$ with higher $\Delta P_{\mathrm{valid}}$. In the case of the TC calculated with $\mathbf{J}^{\mathrm{III}}_Q$, the deviation in the TC is larger than 0.02 $\mathrm{Wm^{-1}K^{-1}}$. The plots in Fig. 3 indicate that when $\Delta P_{\mathrm{valid}}$ is larger, errors in TC become larger and sometimes result in significant deviations.

The good agreement with the reference values suggests that stress training plays a crucial role as anticipated. For EFP-fit, all $|\kappa^{\mathrm{ANN}} - \kappa^{\mathrm{EIP}}|$ calculated with $\mathbf{J}^{\mathrm{I}}_Q$ is plotted near the origin as shown in Fig. 3. There are no cases showing larger TC errors as seen in the EF-fit. The maximum value of $|\kappa^{\mathrm{ANN}} - \kappa^{\mathrm{EIP}}|$ is $\sim$0.005 W $\mathrm{m^{-1}K^{-1}}$, which is much smaller than even the minimum values of $|\kappa^{\mathrm{ANN}} - \kappa^{\mathrm{EIP}}|$ calculated with $\mathbf{J}^{\mathrm{II}}_Q$ and $\mathbf{J}^{\mathrm{III}}_Q$, i.e. 0.055 and 0.041 W $\mathrm{m^{-1}K^{-1}}$, respectively.

From the above results, only $\mathbf{J}^{\mathrm{I}}_Q$ gives a correct estimation of TC. Further, the correct TC may not be obtained even with $\mathbf{J}^{\mathrm{I}}_Q$ unless $\Delta P_{\mathrm{valid}}$ is sufficiently minimized through stress training.

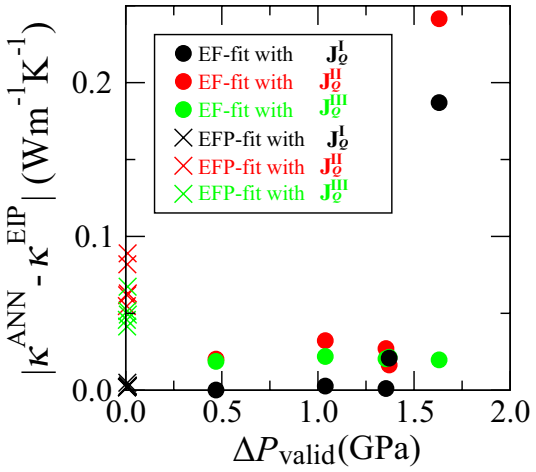

Figure 3: Absolute difference between the TC calculated from the ANN potentials (κ^{ANN}) and the EIP (κ^{EIP}) as a function of root mean square errors for the validation data ($\Delta P_{\mathrm{valid}}$) of five ANN potentials belonging EF-fit (filled circles) and EFP-fit (cross marks) for the validation data. κ^{ANN} and κ^{EIP} are calculated from HNEMD simulations. κ^{ANN} are computed using heat flux formulae $\mathbf{J}^{\mathrm{I}}_Q$ (black), $\mathbf{J}^{\mathrm{II}}_Q$ (red), and $\mathbf{J}^{\mathrm{III}}_Q$ (green). Taken from Ref. [5].

4 Summary

In this report, we have investigated and discussed issues that are unverified with the current training method of MLIPs. Specifically, we reported that the stress training is necessary to accurately reproduce the solid-liquid phase transition of Na and the TC of α-Ag_2Se. In addition, it was suggested that in order to construct more accurate MLIPs from the viewpoint of free energy calculations, increasing the number of k points is not the only solution, and a large-scale system is also necessary.

We would like here to comment on other unestablished aspects of MLIP training methods. It is important to recognize that adjusting the coefficients of the cost function can dramatically alter the accuracy of MLIPs [14]. The heat flux regularization method [31] introduced into the cost-function to estimate partial TCs may also lead to improved robustness of MLIPs. It should be emphasized that more attention should be paid to the importance of the modification of the cost function for the improvement of MLIPs as well as the developments in their architectures and descriptors.

Ackwnowledgements

This study was supported by MEXT/JSPS KAKENHI Grant Numbers Nos. 22K03454, 21H01766, and 19K14676, and JST CREST Grant Number JPMJCR18I2, Japan. The authors thank the Supercomputer Center, the Institute for Solid State Physics, University of Tokyo for the use of the facilities. The computations were also carried out using the facilities of the Research Institute for Information Technology, Kyushu University.

References

[1] Morawietz T and Artrith N 2021 *J. Comput. Aided Mol. Des.* **35** 557–586

[2] Misawa M, Fukushima S, Koura A, Shimamura K, Shimojo F, Tiwari S, Nomura K i, Kalia R K, Nakano A and Vashishta P 2020 *J. Phys. Chem. Lett.* **11** 4536–4541

[3] Yang M, Bonati L, Polino D and Parrinello M 2022 *Catal. Today* **387** 143–149

[4] Irie A, Fukushima S, Koura A, Shimamura K and Shimojo F 2021 *J. Phys. Soc. Jpn* **90** 094603

[5] Shimamura K, Takeshita Y, Fukushima S, Koura A and Shimojo F 2021 *Chem. Phys. Lett.* **778** 138748

[6] Behler J 2021 *Chem. Rev.* **121** 10037–10072

[7] Fukushima S, Ushijima E, Kumazoe H, Koura A, Shimojo F, Shimamura K, Misawa M, Kalia R K, Nakano A and Vashishta P 2019 *Phys. Rev. B* **100**(21) 214108

[8] Fan Z, Pereira L F C, Wang H Q, Zheng J C, Donadio D and Harju A 2015 *Phys. Rev. B* **92**(9) 094301

[9] Shimamura K, Takeshita Y, Fukushima S, Koura A and Shimojo F 2020 *J. Chem. Phys.* **153** 234301

[10] Shimojo F, Fukushima S, Kumazoe H, Misawa M, Ohmura S, Rajak P, Shimamura K, Bassman L, Tiwari S, Kalia R K, Nakano A and Vashishta P 2019 *SoftwareX* **10** 100307

[11] Artrith N and Urban A 2016 *Comput. Mater. Sci.* **114** 135 – 150

[12] Behler J and Parrinello M 2007 *Phys. Rev. Lett.* **98**(14) 146401

[13] Artrith N, Urban A and Ceder G 2017 *Phys. Rev. B* **96**(1) 014112

[14] Irie A, Shimamura K, Koura A and Shimojo F 2022 *J. Phys. Soc. Jpn.* **91** 045002

[15] Kresse G and Joubert D 1999 *Phys. Rev. B* **59** 1758–1775

[16] Hohenberg P and Kohn W 1964 *Phys. Rev.* **136** B864

[17] Perdew J P, Burke K and Ernzerhof M 1996 *Phys. Rev. Lett.* **77** 3865–3868

[18] Tuckerman M, Berne B J and Martyna G J 1992 *J. Chem. Phys.* **97** 1990–2001

[19] Rang M and Kresse G 2019 *Phys. Rev. B* **99**(18) 184103

[20] Rino J P, Hornos Y M M, Antonio G A, Ebbsjö I, Kalia R K and Vashishta P 1988 *J. Chem. Phys.* **89** 7542–7555

[21] Shimojo F and Okazaki H 1991 *J. Phys. Soc. Jpn.* **60** 3745–3753

[22] Okazaki H 1967 *J. Phys. Soc. Jpn.* **23** 355–360

[23] Kubo R 1957 *J. Phys. Soc. Jpn.* **12** 570–586

[24] Green M S 1952 *J. Chem. Phys.* **20** 1281–1295

[25] Behler J 2011 *J. Chem. Phys.* **134** 074106

[26] Mangold C, Chen S, Barbalinardo G, Behler J, Pochet P, Termentzidis K, Han Y, Chaput L, Lacroix D and Donadio D 2020 *J. Appl. Phys.* **127** 244901

[27] Sosso G C, Donadio D, Caravati S, Behler J and Bernasconi M 2012 *Phys. Rev. B* **86**(10) 104301

[28] Surblys D, Matsubara H, Kikugawa G and Ohara T 2019 *Phys. Rev. E* **99**(5) 051301

[29] Boone P, Babaei H and Wilmer C E 2019 *J. Chem. Theory Comput.* **15** 5579–5587

[30] Evans D J 1982 *Phys. Lett. A* **91** 457 – 460

[31] Shimamura K, Koura A and Shimojo F 2022 *arXiv*: 2101.10468